

# Reconstruction of Optical Schrödinger Kitten States Solely with Continuous Variable Field Measurements

H. M. Chrzanowski,<sup>1,2</sup> J. Bernu,<sup>1,2</sup> B. M. Sparkes,<sup>1,2</sup> B. Hage,<sup>1,2</sup>  
A. Lund,<sup>1,3</sup> T. C. Ralph,<sup>1,4</sup> P. K. Lam\*,<sup>1,2</sup> and T. Symul<sup>1,2</sup>

<sup>1</sup>Centre for Quantum Computation and Communication Technology

<sup>2</sup>Quantum Optics group, Department of Quantum Science, Research School of Physics and Engineering,  
Australian National University, Canberra ACT 0200, Australia.

<sup>3</sup>Centre for Quantum Dynamics, Griffith University, Nathan QLD 4111, Australia.

<sup>4</sup>Department of Physics, University of Queensland, St. Lucia QLD 4072, Australia.

The Schrödinger Cat *gedankenexperiment*, which considers the quantum superposition of the dead and alive states of a household pet, is a quintessential example of the enigmatic nature of quantum physics [1]. Optical Schrödinger cats, commonly defined as the quantum superposition of two classically distinguishable coherent states, have applications in quantum communications [2, 3], metrology [4, 5] and quantum computing [6–8]. To deterministically generate such states requires extreme nonlinearity with negligible losses. An alternative to this experimental difficulty is to introduce non-Gaussian post-selective measurements. For example, photon-counting can be exploited to conditionally herald non-Gaussian states, while field measurements are subsequently used to characterise them [9–16]. These ‘hybrid’ experiments face the challenges arising from simultaneously measuring both the wave and particle properties of light. In this letter, we demonstrate a method to reconstruct non-Gaussian states solely with continuous variable field measurements. We show the versatility of this technique by experimentally reconstructing one, two and three photon subtracted squeezed vacuum states.

Historically, quantum optics experiments have been performed in two different kinds of setups, each exploiting only one aspect of the wave-particle duality of light. The “Discrete Variable” (DV) approach relies on quantized measurements of optical systems with low photon numbers. In contrast, the “Continuous Variable” (CV) approach focuses on field measurements of comparatively bright beams. Recently “hybrid” setups that combine DV photon counting and CV homodyne detection, have successfully exploited measurement-induced nonlinearity and tomographic characterization to reconstruct non-Gaussian quantum states [9–16].

As an example, a good approximation of small Schrödinger Cat states, so-called Schrödinger Kitten states [11], can be prepared by subtracting photons from a squeezed vacuum state [17]. Probabilistic photon subtraction can be well approximated experimentally by reflecting a small portion of the beam towards a photon counter; the detection of  $k$  photons heralding the correctly prepared  $k$ -Photon Subtracted Squeezed Vac-

uum state ( $k$ -PSSV). The Wigner functions [18] of the 1-PSSV [11–13] and 2-PSSV [13, 16] states have been experimentally observed, with negative values indicating the non-classicality of the reconstructed state.

In this letter, we present an alternative to reconstruct Schrödinger kitten states using only linear optics and homodyne detection. CV techniques combined with linear optics are known to be insufficient to prepare non-Gaussian states with negativity in their Wigner functions. Nevertheless, the idea of measuring the corpuscular nature of light with only CV techniques has been theoretically [19, 20] and experimentally [21, 22] investigated. Here we extend these ideas and show how DV heralding can be replaced by pure CV conditioning for the reconstruction of non-Gaussian states. This protocol avoids experimental issues arising from ‘hybridising’ a setup [16]. Although Schrödinger kittens are not heralded, remarkably we can still extract their quantum statistics. Using this method, we have successfully reconstructed 1, 2 and 3-PSSV states.

We first consider the 1-PSSV. A beam splitter is used to divert a small portion of an input squeezed vacuum (mode  $a$ ) for conditioning whilst the remainder (mode  $b$ ) is sent to a CV tomographic detector that measures  $\hat{X}_b^\theta = e^{-i\theta}\hat{a}_b + e^{i\theta}\hat{a}_b^\dagger$ , where  $\hat{a}_b$  and  $\hat{a}_b^\dagger$  are the annihilation and creation operators in mode  $b$  and  $\theta$  is the quadrature angle. In hybrid experiments (see Fig.1(i)) the probability distributions of the 1-PSSV states are experimentally estimated by reconstructing histograms of  $X_b^\theta$  only when a single photon is detected in mode  $a$ . The CV-only protocol presented here (see Fig.1(ii)) replaces the DV conditioning with a dual-homodyne measurement. Simultaneously measuring conjugate quadratures must pertain to photon counting given the relation between the photon number and field operators

$$\hat{n}_a = \hat{a}_a^\dagger \hat{a}_a = \frac{1}{4} \left[ (\hat{X}_a^+)^2 + (\hat{X}_a^-)^2 - 2 \right], \quad (1)$$

where  $\hat{X}_a^+ = \hat{X}_a^{\phi=0}$  and  $\hat{X}_a^- = \hat{X}_a^{\phi=\pi/2}$ , or any other pair of orthogonal quadratures  $\hat{X}_a^\phi$  and  $\hat{X}_a^{\phi+\pi/2}$ . Perfect simultaneous measurement of  $\hat{X}_a^+$  and  $\hat{X}_a^-$  is, however, forbidden by Heisenberg’s inequality. Attempts to simultaneously sample these conjugate observables, by splitting  $a$  into two modes  $a1$  and  $a2$  and implementing a dual-homodyne detection, incur a noise penalty in the form

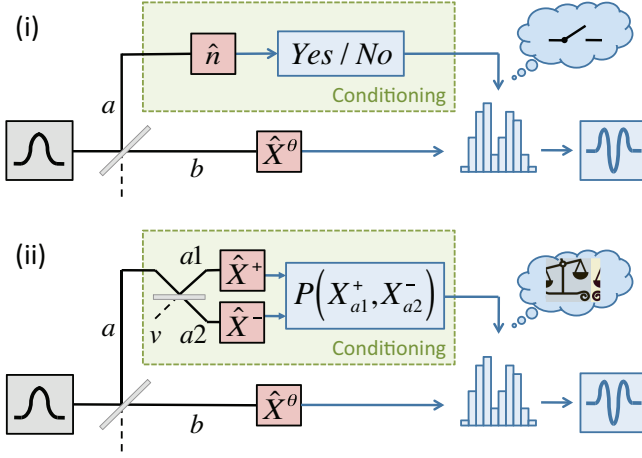


FIG. 1: **Schematic of  $k$ -photon subtracted squeezed vacuum states reconstruction.** Both schemes require squeezed Gaussian input states. A beam-splitter is used to tap-off a small portion of the input beam,  $a$ , for conditioning measurement. The remaining light,  $b$ , is analysed with tomographic measurements. (i) **Hybrid Setup:** outcomes from photon number resolving detectors are used to gate the results of the tomographic detection. Keeping only the conditionally heralded statistics, non-Gaussian quantum states are reconstructed; (ii) **Pure Continuous Variable Setup:** simultaneous orthogonal quadrature measurements are performed to weight the statistics of the tomographic measurements, producing non-Gaussian statistics.

of vacuum fluctuations entering the empty input port  $v$  of the beam-splitter (see Fig.1(ii)). As a consequence, attempts to measure  $n_a$  by using dual homodyne detection produce continuous real values rather than integer results. Using this ‘vacuum polluted’ outcome for single shot heralding, as done in hybrid experiments, would lead to meaningless results. However, treating the measurements as a whole ensemble and using the results of our conditioning measurement of  $X_{a1}^+$  and  $X_{a2}^-$  as a weighting for  $X_b^\theta$ , this additional noise contribution can be removed upon averaging. As the statistical properties of the vacuum noise are perfectly known, the ideal polynomial of  $\hat{X}_a^+$  and  $\hat{X}_a^-$  given by Eq. (1) can be transformed into another polynomial  $[(\hat{X}_{a1}^+)^2 + (\hat{X}_{a2}^-)^2 - 2]/2$  that achieves, on average, the same weighting. We use the resulting weighted contributions of  $X_b^\theta$  to estimate the probability distributions of the 1-PSSV state (see Methods for detailed discussion).

To understand why such a protocol produces the statistics of a 1-PSSV state, we note that weighting upon  $n_a$  can be considered as eliminating contributions of  $X_b^\theta$  corresponding to  $n_a = 0$  (*i.e.* no photon subtraction), and retaining the desired contributions where  $n_a = 1$  (*i.e.* successful photon subtraction).

This idea can be extended to more sophisticated polynomials  $P(\hat{n}_a)$ , permitting us to reconstruct purer and/or larger  $k$ -PSSV states. Larger  $k$ -PSSV states can be reconstructed using polynomials that remove the contribu-

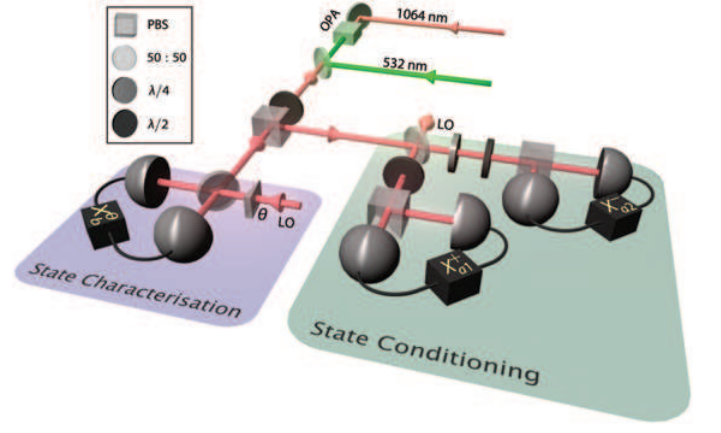


FIG. 2: **Experimental set-up for the pure CV protocol.** A squeezed vacuum state ( $V_s = -3.78$  dB of squeezing for  $V_a = +4.33$  dB of antisqueezing) at the sideband frequencies around 4 MHz of a bright carrier is produced by a degenerate optical parametric amplifier (OPA) [23]. A variable beam splitter, a  $\lambda/2$  wave plate combined with a polarising beam splitter (PBS), reflects 20% of the incoming beam for conditioning and transmits the remaining for tomographic reconstruction. The conditioning beam is split between two homodyne detections (channels  $a_1$  and  $a_2$ ) measuring two arbitrary orthogonal quadratures  $X_{a1}^\phi$  and  $X_{a2}^{\phi+\frac{\pi}{2}}$ . The orthogonality between the homodyning angles for modes  $a_1$  and  $a_2$  is set using a combination of polarisation optics [24], whilst the global phase  $\phi$  does not require active control (see eqn.1). The tomographic reconstruction is performed by sampling  $X_b^\theta$  at 12 fixed angles  $\theta$  between 0 and  $180^\circ$  in intervals of  $15^\circ$ .

tions associated with subtracted photon numbers smaller than  $k$ , and keep outcomes corresponding to  $n_a = k$  as the predominant contribution. For example, the 2-PSSV state can be reconstructed using  $P(\hat{n}_a) = \hat{n}_a(\hat{n}_a - 1)$ , removing contributions resulting from having 0 or 1 photon in mode  $a$ . We can also apply the same technique to remove contributions corresponding to unwanted higher order photon number subtractions contaminating the weighted ensemble. If we consider the simplest  $P(\hat{n}_a) = \hat{n}_a$  conditioning polynomial to reconstruct the 1-PSSV, whilst contributions corresponding to  $n_a = 0$  are cancelled, measurements associated with two photon subtraction are kept, and their statistical contribution is weighted at 2. As a result the reconstructed state is a statistical mixture of the 1-PSSV with some contribution from the 2-PSSV. These two states display out of phase interference fringes, resulting in a partial wash-out of the negativity of the reconstructed Wigner function. However, using  $P(\hat{n}_a) = \hat{n}_a(\hat{n}_a - 2)$  for conditioning allows us to remove contributions resulting from having 0 or 2 photons in mode  $a$ . These two conditioning techniques can, in theory, be extended to an arbitrary order allowing a CV analog to the DV photon number resolving detector.

Our experimental setup is detailed in Fig.2. Great care was taken to match the electronic response of all

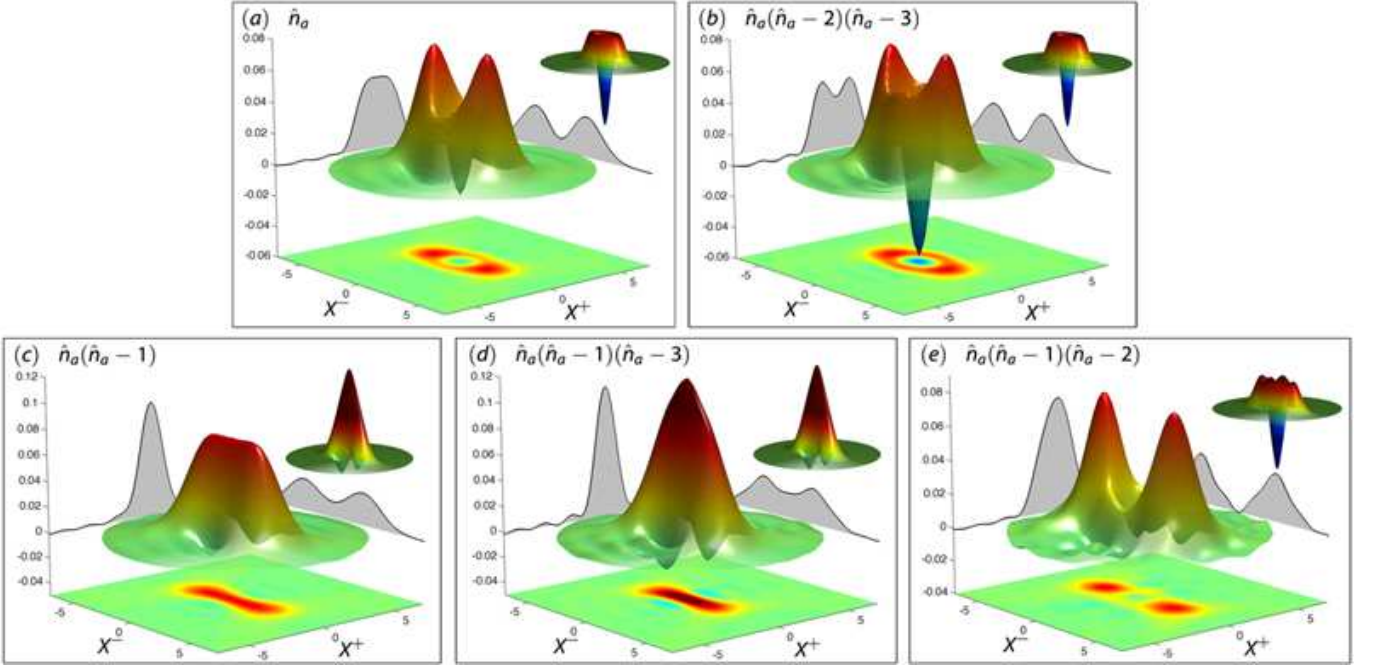


FIG. 3: Wigner Functions reconstructed via the inverse Radon transform. The specific weighting polynomial is given at the top of each diagram. **1-PSSV**: (i) without and (ii) with higher order correction respectively, showing a improvement in the negativity from  $-0.018$  to  $-0.055$  compared to  $-0.16$  in the ideal case. **2-PSSV**: (iii) without and (iv) with higher order correction respectively. It shows an improvement in the size of the central positive fringes (and first negative fringe) from  $+0.077$  ( $-0.011$ ) to  $+0.122$  ( $-0.023$ ) compared to  $+0.16$  ( $-0.03$ ) in the ideal case. **3-PSSV**: without (v) higher order correction, showing a central fringe with a negativity of  $-0.004$  compared to  $-0.16$  in the ideal case. The insets display the corresponding calculated 1, 2 and 3-PSSV states assuming pure initial squeezed states and ideal photon subtraction.

three homodyne detectors to preserve the correlations between the conditioning and characterisation modes. All of the presented Wigner functions (Fig.3) are reconstructed directly from the probability distributions obtained by applying various conditioning polynomials to a unique dataset. This dataset is composed of approximately 1.2 billion samples for each detection mode and for each of the 12 tomographic angles. Whilst some reconstruction methods require assumptions on the nature of the state, the inverse Radon transform [18] used here is direct and assumption free. Moreover we do not correct for any experimental inefficiencies.

Fig.3(i) shows the Wigner function obtained using the conditioning polynomial  $P(\hat{n}_a) = \hat{n}_a$ , and displays a clear negativity. Our protocol, however, relies on correlations between modes  $a1$ ,  $a2$  and  $b$ , which are affected by any process that adds extra uncorrelated classical or quantum fluctuations. The primary limitation is the finite purity of our squeezed vacuum resource, that can be modelled as an effective loss of  $\sim 12\%$  applied on a pure squeezed state. We note that this non-ideal resource is also a limiting factor in hybrid experiments [16]. Another possible limitation comes from the finite homodyne efficiency and dark noise. The dark noise, analogous to the dark counts of DV detectors, is at least 22 dB smaller than the vacuum fluctuations. Our homodyne efficiency is limited by the quantum efficiency of the detectors, estimated at

between 93-96%, whilst mode matching efficiency is typically greater than 99%. In contrast, hybrid experiments suffer a substantial loss contribution from the difficulty in isolating the correct spatio-temporal mode in the conditioning and characterisation stages. Finally, the need for a finite conditioning tap-off and squeezing inevitably introduces spurious higher order photon subtraction contributions in the reconstructed state. By using the conditioning polynomial  $P(\hat{n}_a) = \hat{n}_a(\hat{n}_a - 2)(\hat{n}_a - 3)$ , the contributions from 2 and 3 photon subtractions are removed; the further higher orders being negligible. As expected, Fig.3(ii) shows a considerable improvement in the negativity of the reconstructed 1-PSSV state.

Fig.3(iii) shows the 2-PSSV obtained using  $P(\hat{n}_a) = \hat{n}_a(\hat{n}_a - 1)$ . The reconstructed state exhibits the expected central positive fringe and two negative side fringes, as well as a bigger separation of the two coherent components [17]. As shown in Fig.3(iv), correcting for higher order contaminations by using  $P(\hat{n}_a) = \hat{n}_a(\hat{n}_a - 1)(\hat{n}_a - 3)$  enhances the purity of the 2-PSSV state, evidenced by an improvement in the size of the fringes.

Finally, reconstructing the 3-PSSV state is extremely challenging as the likelihood of obtaining three photons at the conditioning stage is minute. We combated this challenge by optimising the conditioning tap-off, the squeezing parameter, as well as recording a large dataset, in order to achieve a good compromise



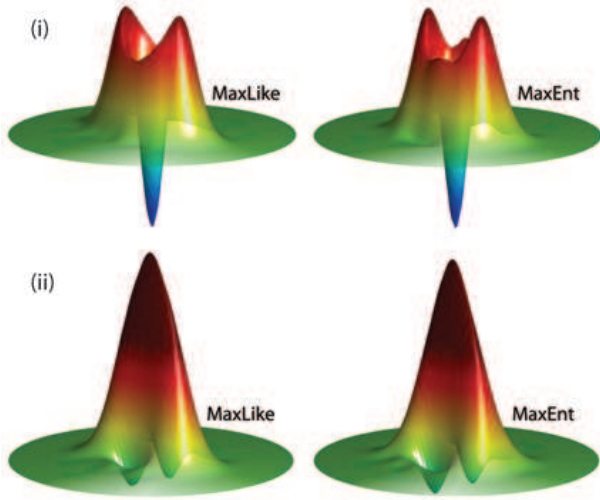


FIG. 4: Wigner Function of the higher order corrected (i) 1-PSSV and (ii) 2-PSSV reconstructed via two other assumption free methods. Maximum Likelihood (MaxLike) as defined in [25], and maximum Entropy (MaxEnt) [26]. Both methods of reconstruction use a density matrix dimension of 20 photons squared.

between statistical relevance and purity of the reconstructed state (see Methods). The reconstruction using  $P(\hat{n}_a) = \hat{n}_a(\hat{n}_a - 1)(\hat{n}_a - 2)$  displayed in Fig.3(v) shows a further improvement in the ‘dead-and-alive’ separation. The purity of the reconstructed state is largely limited by higher order contaminations, as predicted by our models. Correcting for these unwanted contributions requires a higher degree polynomial of  $\hat{n}_a$ . The amount of data needed to efficiently average out the vacuum fluctuations entering mode  $v$  grows rapidly with the degree of the conditioning polynomial (see Methods). With our finite dataset size, the residual statistical noise was larger than the weak signal of interest, preventing us from achieving

the desired purification.

Fig.4 shows the Wigner functions of the higher order corrected 1-PSSV and 2-PSSV states obtained using the *MaxEnt* [26] and *MaxLike* [9] algorithms without any assumption on the nature of the state. The reconstructed Wigner functions are qualitatively identical to those produced by the Radon transformation, reinforcing that the quantum features observed are intrinsic to our experimental data.

We have demonstrated a technique to reconstruct conditional non-Gaussian states using only Gaussian resources, linear optics and homodyne detection. Our technique can be extended to test other quantum information protocols relying on similar hybrid, or ‘de-Gaussification’, techniques. By avoiding direct photon-counting, we circumvented the difficulties arising from simultaneously exploiting the wave and particle nature of light, permitting us to unambiguously reconstruct up to the 3-PSSV. We observed negativities in all of the reconstructed Wigner functions, independent of the reconstruction algorithm used.

#### Acknowledgment:

We thank E. Huntington for useful discussions. This research was conducted by the *Australian Research Council Centre of Excellence for Quantum Computation and Communication Technology* (project number CE110001029).

#### Author contributions

T.S. and P.K.L. planned and supervised the project. H.M.C. and T.S. conducted the experiment. J.B., T.S. and B.H. developed the experimental model and analysis. A.L. and T.C.R. proposed the original theoretical model. B.M.S and T.S. developed the universal FPGA based digital locking system used to control the experiment [27]. All authors discussed the results and commented on the manuscript at all stages.

- 
- [1] Schrödinger, E. *Naturwissenschaften* **23**, 807 (1935); **23**, 823 (1935); **23**, 844 (1935).
  - [2] Cochrane, P., Milburn, G. J. and Munro, W.J., Macroscopically distinct quantum-superposition states as a bosonic code for amplitude damping. *Phys. Rev. A* **59**, 2631 (1998).
  - [3] Ourjoumtsev, A., Ferreyrol, F., Tualle-Broui, R. and Grangier, P., Preparation of non-local superpositions of quasi-classical light states. *Nature Physics* **5**, 189 (2009).
  - [4] Ralph, T.C., Coherent Superposition States as Quantum Rulers. *Phys. Rev. A* **65**, 042313 (2002).
  - [5] Gilchrist, A., Nemoto, K., Munro, W. J., Ralph, T. C., Glancy, S., Braunstein, S. L., Milburn, G. J., Schrödinger cats and their power for quantum information processing. *J. Opt. B* **6**, S828 (2004).
  - [6] Ralph, T. C., Gilchrist, A., Milburn, G. J., Munro, W. J. and Glancy, S. Quantum computation with optical coherent states. *Phys. Rev. A* **68**, 042319 (2003).
  - [7] Jeong, H., Kim, M. S. Efficient quantum computation using coherent states. *Phys. Rev. A* **65**, 1-6 (2002).
  - [8] Lund, A.P., Ralph, T. C. and Haselgrove, H. L., Fault-Tolerant Linear Optical Quantum Computing with Small-Amplitude Coherent States. *Phys. Rev. Lett.* **100**, 030503 (2008).
  - [9] Lvovsky, A. I., Hansen, H., Aichele, T., Benson, O., Mlynek, J. and Schiller, S., Quantum State Reconstruction of the Single-Photon Fock State. *Phys. Rev. Lett.* **87**, 50402 (2001).
  - [10] Ourjoumtsev, A., Tualle-Broui, R. and Grangier, P., Quantum homodyne tomography of a two-photon Fock state. *Phys. Rev. Lett.* **96**, 213601 (2006).
  - [11] Ourjoumtsev, A., Tualle-Broui, R., Laurat, J. and Grangier, P. Generating Optical Schrodinger Kittens for Quantum Information Processing. *Science* **312**, 83-86 (2006).
  - [12] Neergaard-Nielsen, J. S., Nielsen, B. M., Hettich, C.,

- Mölmer, K. and Polzik, E.S., Generation of a superposition of odd photon number states for quantum information networks. *Phys. Rev. Lett.* **97**, 833604 (2007).
- [13] Wakui, A., Takahashi, H., Furusawa, A. and Sasaki, M., Photon subtracted squeezed states generated with periodically poled KTiOPO4. *Opt. Express* **15**, 3568-3574 (2007).
- [14] Ourjoumtsev, Jeong, H., Tualle-Broui, R. and Grangier, P., Generation of optical ‘Schrodinger cats’ from photon number states. *Nature* **448**, 784-786 (2007).
- [15] Parigi, V., Zacatta, A., Kim, M. and Bellini, M. Probing quantum commutation rules by addition and subtraction of single photons to/from a light field. *Science* **317**, 1890 (2007).
- [16] Namekata, N., Takahashi, Y., Fujii, G., Fukuda, D., Kuimura, S. and Inoue, S., Non-Gaussian operation based on photon subtraction using a photon-number-resolving detector at a telecommunications wavelength. *Nature Photonics* **4** 655-660 (2010).
- [17] Dakna, M., Anhut, T., Opatrny, T., Knöll, L. and Welsch, D. G. Generating Schrödinger-cat-like states by means of conditional measurements on a beam splitter. *Phys. Rev. A* **55**, 3184-3194 (1997).
- [18] Leonhardt, U., Measuring the Quantum State of Light (Cambridge University Press, Cambridge, 1997).
- [19] Ralph, T. C., Munro, W. J. and Polkinghorne, R. E. S., Proposal for the Measurement of Bell-like Correlations from Continuous Variables. *Phys. Rev. Lett.* **85**, 2035 (2000).
- [20] Ralph, T. C., Huntington, E. H. and Symul, T., Single-photon side bands. *Phys. Rev. A* **77**, 063817 (2008).
- [21] Webb, J. G., Ralph, T. C. and Huntington, E. H., Homodyne measurement of average photon number. *Phys. Rev. A* **73**, 033808 (2006).
- [22] Grosse, N. B., Symul, T., Stobinska, M., Ralph, T. C. and Lam, P. K., Measuring photon anti-bunching from continuous variable sideband squeezing. *Phys. Rev. Lett.* **98**, 153603 (2007).
- [23] Stefszky, M., Mow-Lowry, C. M., McKenzie, K., Chua, S., Buchler, B. C., Symul, T., McClelland, D. E. and Lam, P. K. An investigation of doubly-resonant optical parametric oscillators and nonlinear crystals for squeezing. *J. Phys. B: At. Mol. Opt. Phys.* **44** 015502 (2010).
- [24] Lance, A.M., Symul, T., Sharma, V., Weedbrook, C., Ralph, T.C. and Lam, P.K., No-Switching Quantum Key Distribution Using Broadband Modulated Coherent Light, *Phys. Rev. Lett.* **95** 180503 (2005).
- [25] Lvovsky, A. I., Iterative maximum-likelihood reconstruction in quantum homodyne tomography. *J. Opt. B* **6** S556 (2004).
- [26] Buzek, V. and Drobny, G., Quantum tomography via the MaxEnt principle *J. Mod. Opt.*, **47**, 2823 (2000).
- [27] see <http://photonics.anu.edu.au/qoptics/index.html> for details and code.

**Methods: From DV photoncounting conditioning to CV dual homodyne weighting.** From a hybrid experiment point of view, the probability distributions of the quadrature  $x_b^\theta$  for the  $k$ -PSSV are defined as

$$p(x_b^\theta) \equiv p(X_b^\theta = x | n_a = k). \quad (2)$$

These are experimentally estimated by constructing conditioned histograms: with sufficiently small bin size and a statistically relevant ensemble, we approximate

$$p(x_b^\theta) = \langle \chi_x(\hat{X}_b^\theta) \rangle_{n_a=k} \quad (3)$$

where  $\langle \dots \rangle_{n_a=k}$  denotes the mean value conditioned upon  $n_a = k$  and  $\chi_x$  denotes the characteristic function of bin  $x$  ( $\chi_x$  is 1 in bin  $x$  and 0 elsewhere). As explained in the main text, conditioning upon  $n_a = k$  can be well approximated by weighting upon a judiciously chosen polynomial  $P(n_a)$  that cancels all significant contributions corresponding to  $n_a \neq k$ :

$$p(x_b^\theta) = \langle \chi_x(\hat{X}_b^\theta) \cdot P(\hat{n}_a) \rangle. \quad (4)$$

Using (1), we rewrite  $P(\hat{n}_a)$  as  $P(\hat{X}_a^+, \hat{X}_a^-)$  and transform it into a polynomial  $Q(\hat{X}_{a1}^+, \hat{X}_{a2}^-)$  realising the same weighting on average:

$$\langle \chi_x(\hat{X}_b^\theta) \cdot Q(\hat{X}_{a1}^+, \hat{X}_{a2}^-) \rangle = \langle \chi_x(\hat{X}_b^\theta) \cdot P(\hat{X}_a^+, \hat{X}_a^-) \rangle \quad (5)$$

hence giving:

$$p(x_b^\theta) = \langle \chi_x(\hat{X}_b^\theta) \cdot Q(\hat{X}_{a1}^+, \hat{X}_{a2}^-) \rangle. \quad (6)$$

This last expression means that  $p(x_b^\theta)$  can be estimated by reconstructing histograms where each contribution  $\hat{X}_b^\theta$  is weighted by the corresponding value of  $Q(\hat{X}_{a1}^+, \hat{X}_{a2}^-)$ .

**Polynomial transformation.** The  $Q(\hat{X}_{a1}^+, \hat{X}_{a2}^-)$  are not trivial to obtain due to non commuting algebra. The demonstration of the existence of  $Q$  for any  $P(\hat{n}_a)$ , and algorithms to compute it, will be published elsewhere. Here we give a few examples:

$$\hat{n}_a \rightarrow \hat{\rho}^2 - 1 \quad (7)$$

$$\hat{n}_a(\hat{n}_a - 1) \rightarrow \hat{\rho}^4 - 4\hat{\rho}^2 - 1 \quad (8)$$

$$\hat{n}_a(\hat{n}_a - 2)(\hat{n}_a - 3) \rightarrow \hat{\rho}^6 - 11\hat{\rho}^4 + 28\hat{\rho}^2 - 12 \quad (9)$$

where we defined  $\hat{\rho}^2 = [(\hat{X}_{a1}^+)^2 + (\hat{X}_{a2}^-)^2]/2$ . Note that all polynomials are only dependant on  $\hat{\rho}^2$ .  $\hat{\rho}^2$  is only critically dependent on the phase space vectorial ‘length’ of  $(\hat{X}_{a1}^+, \hat{X}_{a2}^-)$ , which relates to the energy shared in modes  $a1$  and  $a2$  and hence  $\hat{n}_a$ . This confirms that the global phase  $\phi$  of the dual-homodyne detection is irrelevant, so long as a ‘conjugate’ pair,  $(\hat{X}_{a1}^\phi$  and  $\hat{X}_{a2}^{\phi+\pi/2})$ , is simultaneously measured.

Let us now consider in more detail the 1-PSSV reconstruction, as measured in Fig. 3(i), by specifying  $P(\hat{n}_a) = \hat{n}_a$ . We obtain

$$p(x_b^\theta) = \langle \chi_x(\hat{X}_b^\theta) \cdot P(\hat{X}_a^+, \hat{X}_a^-) \rangle \quad (10)$$

with  $P(\hat{X}_a^+, \hat{X}_a^-)$  given by (1). We aim to prove that using the  $Q(\hat{X}_{a1}^+, \hat{X}_{a2}^-)$  defined in (7) instead of  $P(\hat{X}_a^+, \hat{X}_a^-)$  in (10) leads to the same result. Using the 50:50 beam splitter transformation equations

$$\begin{aligned} \hat{X}_{a1}^+ &= (\hat{X}_a^+ + \hat{X}_v^+)/\sqrt{2} \\ \hat{X}_{a2}^- &= (\hat{X}_a^- - \hat{X}_v^-)/\sqrt{2} \end{aligned} \quad (11)$$

we find

$$\langle \chi_x(\hat{X}_b^\theta) \cdot Q(\hat{X}_{a1}^+, \hat{X}_{a2}^-) \rangle = p(x_b^\theta) + \langle \chi_x(\hat{X}_b^\theta) \cdot \hat{\Delta} \rangle \quad (12)$$

where

$$\hat{\Delta} = (\hat{\Delta}^+ + \hat{\Delta}^-)/2 \quad (13)$$

$$\hat{\Delta}^\pm = (\hat{X}_v^\pm)^2 - 1 \pm \hat{X}_a^\pm \hat{X}_v^\pm \pm \hat{X}_v^\pm \hat{X}_a^\pm. \quad (14)$$

We now note that the field fluctuations of the vacuum  $\hat{X}_v^\pm$  are uncorrelated to those of  $\hat{X}_a^\pm$  and  $\hat{X}_b^\theta$  and hence can be averaged out separately in (12), for example  $\langle \chi_x(\hat{X}_b^\theta) \hat{X}_a^+ \hat{X}_v^+ \rangle = \langle \chi_x(\hat{X}_b^\theta) \hat{X}_a^+ \rangle \langle \hat{X}_v^+ \rangle$ . Finally injecting the values  $\langle \hat{X}_v^\pm \rangle = 0$  and  $\langle (\hat{X}_v^\pm)^2 \rangle = 1$  given by quantum theory, we easily find that  $\langle \chi_x(\hat{X}_b^\theta) \cdot \hat{\Delta} \rangle = 0$ , and hence  $p(x_b^\theta) = \langle \chi_x(\hat{X}_b^\theta) \cdot Q(\hat{X}_{a1}^+, \hat{X}_{a2}^-) \rangle$ .

**Experimental considerations** To enable the reconstruction of the 3-PSSV, we need to optimise the experimental parameters to increase the likelihood of having 3 photons in mode  $a$  without sacrificing the quality of the reconstructed state. There are two main parameters we can adjust: the portion of the input mode used for conditioning and the input squeezing level. We generate large squeezing to populate higher order photon pairs. Experimentally, increasing the squeezing level reduces the purity of our squeezed state. Although increasing the reflectivity of the conditioning beam splitter substantially increases the likelihood of 3 photon subtraction, it also reduces the effective squeezing parameter of the reconstructed  $k$ -PSSV, and hence the fidelity with an ideal Schrödinger cat [17]. This also leads to stronger contamination from higher order subtraction. Rejecting these higher order contribution requires extremely large datasets.

**Weighting polynomial degree and finite statistics.** Reconstructing larger  $k$ -PSSV relies on the extraction of finer

correlations between modes  $a1$ ,  $a2$  and  $b$ , and hence requires greater total samples to obtain a given statistical precision. This is analogous to the need for recording more data to extract a given number of less probable  $k$  subtraction events in hybrid experiments.

Note that in the limit of very low squeezing, the 1-PSSV can be reconstructed merely with  $P(\hat{n}_a) = \hat{n}_a$  as the probability for  $n_a > 1$  is insignificant, but using higher order rejections such as  $P(\hat{n}_a) = \hat{n}_a(\hat{n}_a - 2)(\hat{n}_a - 3) \dots$  would theoretically lead to the same result. However, even if the signal to be extracted is identical, we shall see that the degree of the weighting polynomial  $P(\hat{n}_a)$  has a critical statistical effect when dealing with a real finite dataset. The expansion of  $Q(\hat{X}_{a1}^+, \hat{X}_{a2}^-)$  according to (11) produces vacuum fluctuation terms that theoretically average out in (6) leading to (5) and hence (4). With a finite dataset, however, we are also left with additional statistical noise. For a  $P(\hat{n}_a)$  of degree  $d$ , we obtain moments of up to order  $2d$ , such as  $\langle (\hat{X}_v^\pm)^{2d} \rangle$ . With a given dataset size, the statistical error scales as the standard deviation  $\sigma_d$  of  $(\hat{X}_v^\pm)^{2d}$  given by

$$\sigma_d^2 = \langle (\hat{X}_v^\pm)^{4d} \rangle - \langle (\hat{X}_v^\pm)^{2d} \rangle^2 = (4d - 1)!! - (2d - 1)!!^2, \quad (15)$$

where  $n!! = n(n-2)(n-4) \dots$ , which grows super-exponentially with  $d$ :

$$\begin{aligned} \sigma_1 &\simeq 1.4 \\ \sigma_2 &\simeq 9.8 \\ \sigma_3 &\simeq 1.0 \times 10^2 \\ \sigma_4 &\simeq 1.4 \times 10^3 \\ \sigma_5 &\simeq 2.6 \times 10^4. \end{aligned}$$